Journal of Electrical Engineering and Computer (JEECOM)
Vol. 8, No. 1 (2026), DOI: 10.33650/jeecom.v8i1.16680
p-ISSN: 2715-0410; e-ISSN: 2715-6427


# Flower Pollination Algorithm-Based MPPT for PEM Fuel Cells with Interleaved Buck-Boost Converter

**Pressa P. S. Saputra*[1], Zainal Mustakim[1], Heri Ardiansyah[2], Rifqi Firmansyah[3]**
[1] Universitas Muhammadiyah Gresik, Indonesia
[2] Universitas Muhammadiyah Lamongan, Indonesia
[3] State University of Surabaya, Indonesia

**Article Info**

***Article history:***

Received March 2, 2026
Revised April 20, 2026
Accepted April 29, 2026

***Keywords:***

PEMFC
Flower Pollination Algorithm (FPA)
MPPT
Interleaved Buck-Boost Converter

**ABSTRACT**

*This study proposes an enhanced maximum power point tracking (MPPT) strategy for proton exchange membrane fuel cells (PEMFCs) by integrating a Flower Pollination Algorithm (FPA)-based controller with an IBBC (interleaved buck–boost converter). The non-linear behavior of electrochemical properties of PEMFCs pose significant challenges to conventional MPPT techniques, which often struggle to maintain accurate and stable power tracking under varying operating conditions. Many existing approaches rely primarily on properties like as membrane water content, hydrogen pressure and cell temperature to regulate converter operation. Proposed FPA-based MPPT method improves tracking accuracy and dynamic performance in response to changes in membrane water content, hydrogen pressure and temperature. In addition, interleaved buck–boost topology reduces output current ripple and distributes current stress across switching devices, contributing to enhanced efficiency and system stability. Simulation results demonstrate that the proposed strategy achieves faster convergence to the maximum power point, lower steady-state oscillations, and improved power extraction efficiency compared with conventional MPPT methods across diverse PEMFC operating scenarios.*



***Corresponding Author:***
Pressa P. S. Saputra,
Universitas Muhammadiyah Gresik, Sumatra street no.101 GKB, Gresik, 61121, Indonesia
Email: pressa@umg.ac.id

## 1. INTRODUCTION

The The accelerating growth in global energy consumption, particularly electricity derived from fossil fuels, has intensified the transition toward clean and sustainable energy technologies. Proton Exchange Membrane Fuel Cells (PEMFCs) have emerged as a promising solution due to their high conversion efficiency, low operating temperature, compact structure, and rapid start-up capability. By converting hydrogen and oxygen into electricity through an electrochemical process that produces only water as a byproduct, PEMFCs offer an environmentally sustainable alternative for transportation, distributed generation, backup power systems, and hybrid renewable energy applications [1][2][3]. Despite these advantages, PEMFCs exhibit highly nonlinear voltage–current characteristics and strong sensitivity to operating conditions. Variations in load demand, hydrogen pressure, stack temperature, and membrane water content alter the polarization curve and continuously shift the maximum power point (MPP) [4]. Consequently, maintaining operation at the MPP under dynamic conditions remains a critical challenge, as deviations result in reduced efficiency and suboptimal power utilization.

To address this issue, various Maximum Power Point Tracking (MPPT) techniques have been developed to regulate the DC–DC converter interface and ensure continuous operation at the MPP [5][6]. The converter duty cycle is dynamically adjusted by MPPT algorithms to track highest attainable power under changing conditions, similar to strategies employed in photovoltaic systems [7].

Ordinary methods includes Incremental Conductance (IC) and Perturb and Observe (P&O) are frequently chosen due to their simplicity in application. While IC generally provides faster convergence and improved stability under parameter variations compared to P&O [8][9][10], both methods may suffer from steady-state oscillations and degraded tracking performance under rapid dynamic changes.

To better accommodate nonlinear and time-varying system behavior, intelligent and metaheuristic approaches such as Particle Swarm Optimization (PSO), Fuzzy Logic Control (FLC), and hybrid Artificial Bee Colony (ABC)-based schemes have been introduced [11][12][13]. These methods improve convergence characteristics and robustness; however, many existing studies consider limited operating variations and frequently employ conventional boost converter topologies, which may increase current ripple and restrict dynamic performance.

Motivated by these limitations, this paper proposes a MPPT based on the Flower Pollination Algorithm (FPA) combined with an interleaved buck–boost converter (IBBC) for enhanced PEMFC power management. The FPA provides a balanced global–local search mechanism, enabling adaptive and accurate MPP tracking under simultaneous variations in stack temperature and membrane hydration. The algorithm determines the optimal duty cycle to regulate the IBBC, which offers bidirectional voltage control capability and reduced output current ripple through phase interleaving. This topology enhances transient response, distributes stress switching, and improves overall conversion efficiency.

Simulation results demonstrate that the proposed FPA–IBBC configuration achieves faster convergence, lower steady-state oscillations, and improved robustness compared with conventional and metaheuristic MPPT methods under dynamic operating conditions. These findings highlight the effectiveness of combining advanced optimization strategies with improved converter architectures for high-performance PEMFC power regulation.

The remainder of this paper is structured as follows. Section II presents the PEMFC modeling and polarization characteristics. Section III describes the interleaved buck–boost converter topology. Section IV details the proposed FPA-based MPPT strategy. Section V provides simulation outcomes and comparable performance analysis. Finally, Section VI conclusion of paper.

## 2. MODELING OF THE PROPOSED PEMFC SYSTEM

This section presents the PEMFC system integrated with FPA-based MPPT scheme. The overall system configuration, shown in Fig. 1, consists of a PEMFC stack, an interleaved buck–boost converter (IBBC), an FPA-based controller, a pulse-width modulation (PWM) module, and a resistive load.

The FPA controller determines the optimal duty cycle for the IBBC by evaluating the instantaneous output of PEMFC Power, computed from the measured signals of voltage and current. Since the maximum power point (MPP) varies with changes in membrane hydration and operating temperature, the controller adaptively updates the duty cycle to ensure continuous operation at the MPP.

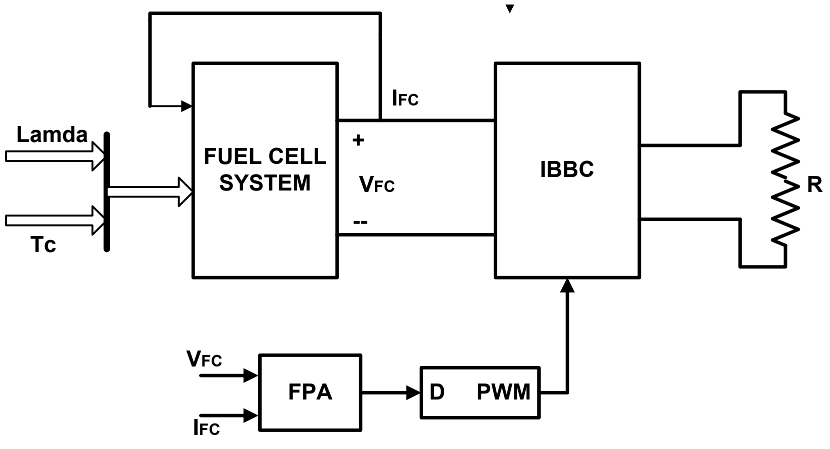


Figure 1. Block diagram of FPA based MPPT

### 2. 1.PEM-Fuel Cell Model

The accurate mathematical modeling is essential to capture both the steady-state and dynamic behavior of the PEMFC system. Such modeling enables systematic performance analysis under varying operating conditions through appropriate parameter adjustments. In this study, the Horizon H-1000 PEMFC is adopted as the reference model, and its manufacturer-specified parameters are utilized to ensure realistic and representative system performance [14]. The key specifications of the PEMFC employed in this work are summarized in Table 1.

Table 1. Constanta of H-1000 PEMFC Type

| No. | Constanta | Value |
|---|---|---|
| 1 | Cell Amount | 72 |
| 2 | Nom. Power | 1000 W |
| 3 | Nom. Volt | 43.2 V |
| 4 | λ | 14 molH2O/molSO$^{3-}$ |
| 5 | Jmax | 1 A.cm$^{-2}$ |
| 6 | A | 56.6 cm$^{2}$ |
| 7 | PH2 | 1.45 atm |
| 8 | PO2 | 1 atm |
| 9 | β1, β2, β3, β4 | -0.9514, 3.12x10$^{-3}$, 7.4x10$^{-5}$, -1.87x 10$^{-4}$ |
| 10 | Tstd | 303°K |

The polarization curve of power–current demonstrate that increases in content of membrane water and PEMFC temperature lead to higher power output of the stack, thereby requiring an effective MPPT strategy to keep maximum operation. As seen in Fig. 2 and 3, variations in temperature and membrane hydration shift the power curve, altering the location of the maximum power point under different loading conditions.

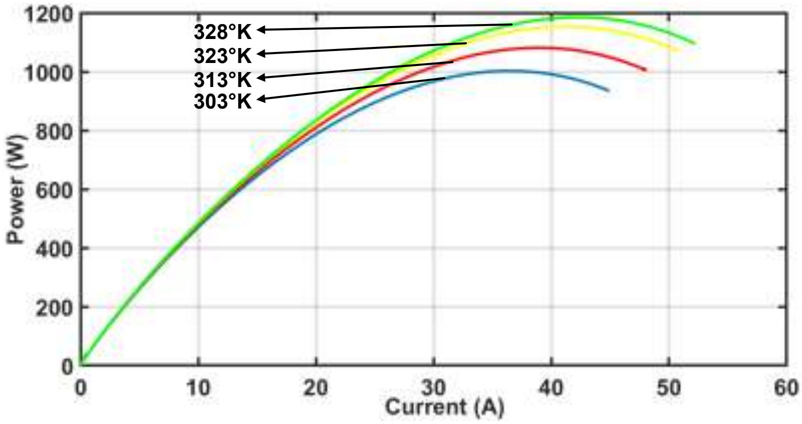


(a)

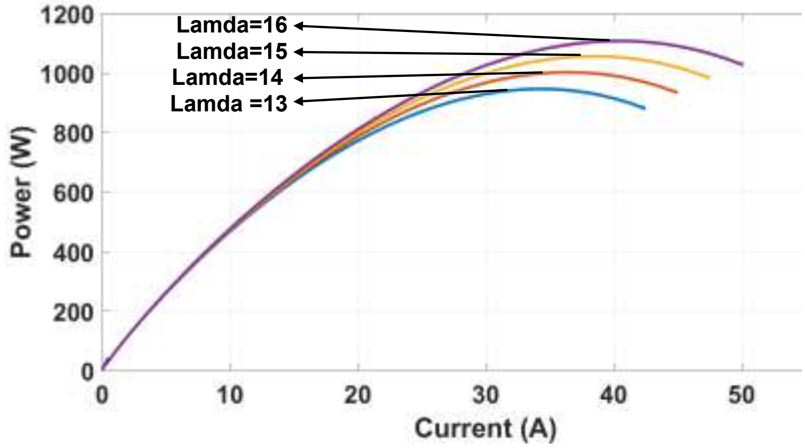


(b)

Figure 2. Current vs Power PEMFC in (a) different temperature, (b) different temperature membrane water content (λ)

The maximum theoretical cell voltage corresponds to the open-circuit condition, where no external current is drawn from the stack. Under this condition, the reversible cell voltage is determined by the Nernst equation, as expressed in Eq. 1 [14][15][16].

$$E_{nernst} = E_0 - \frac{RT}{2F}\ln(P_{H_2} * P_{O_2}^{0.5}) \quad (1)$$

Enerst represents the EMF (electromotive force) of PEMFC based specified temperature and pressure conditions, generally mentioned as the voltage of ideal cell. The potential of standard electrode, E0, is about 1.23 V for formation of liquid water and 1.79 V for the formation of water vapor under standard conditions [17].

## 2. 2. Interleaved Buck-Boost Converter

Figure 3 presents the configuration of the proposed interleaved buck–boost converter (IBBC), which comprises $n$ parallel-connected buck–boost converter cells [18][19]. Each phase operates with a uniform switching frequency and is phase-shifted relative to the others to achieve interleaving. For example, in a two-phase configuration, the gating signals are shifted by 180°, whereas in a four-phase system, a 90° phase displacement is applied. This phase interleaving extends proportionally with the number of phases.

The interleaving mechanism significantly attenuates output current ripple by distributing the switching intervals across phases. The overall output current is obtained as the sum of the individual phase currents, resulting in a smoother combined waveform. Moreover, sharing the load current among multiple phases reduces the current stress on each semiconductor device, thereby enhancing converter reliability and thermal performance [20][21]. The modular structure also improves fault tolerance and scalability, as additional phases can be incorporated or maintained independently without interrupting overall system operation.

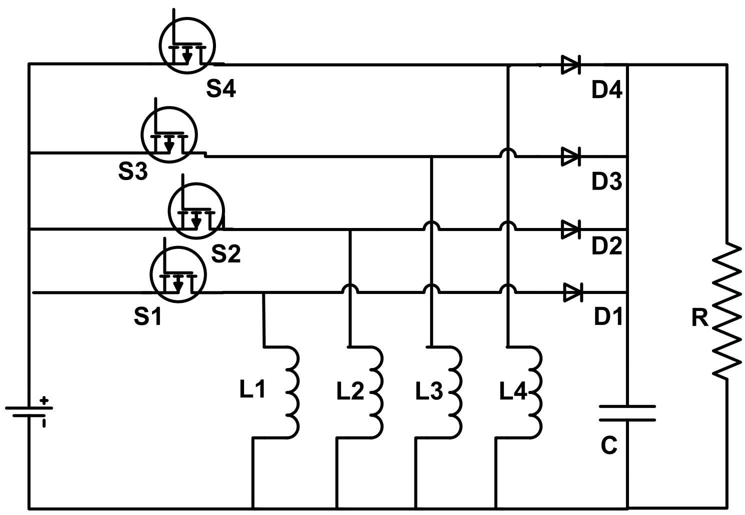


Figure 3. 4-phase interleaved buck boost converter

The proposed converter is made up of four interleaved buck–boost cells, each operating with a uniform switching frequency and a phase displacement of 90°. This configuration generates four phase-shifted gating signals to control the corresponding MOSFET switches. Specifically, the switching sequence is arranged such that the first MOSFET is activated at 0°, followed by the second at 90°, the third at 180°, and the fourth at 270°. Figure 4 depicts the four-phase interleaved topology along with the associated gating waveforms, illustrating the phase-shifted switching pattern applied to each converter cell.

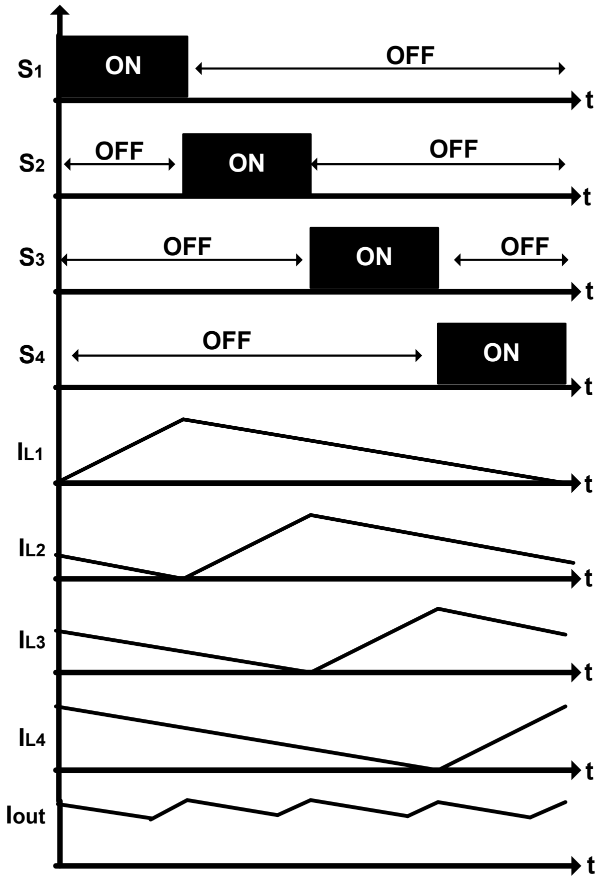


Figure 4. Inductor current profile and switching behavior when a duty cycle

**2. 3. MPPT Based Flower Pollination Algorithm (FPA)**

The FPA is a nature-inspired metaheuristic optimization technique derived from the biological process of flower pollination [22][23][24]. In natural ecosystems, pollination refers to the transfer of pollen between flowers to enable reproduction. This process can be classified into two primary mechanisms: self-pollination (abiotic), which occurs within the same plant or species, and cross-pollination (biotic), which involves pollen transfer between different plants facilitated by external agents such as insects, birds, or other pollinators.

Empirical observations indicate that cross-pollination dominates in nature, accounting for approximately 91% of pollination activities, whereas auto-pollination represents a smaller proportion. In the FPA framework, these two mechanisms are mathematically modeled as global and local search processes, respectively. The transition between global (cross-pollination) and local (self-pollination) search is governed by a switch probability parameter ($p \in [0,1]$). The algorithm implementation follows several fundamental rules, as summarized below [25][26][27]

**Rule 1**:

Biotic or cross-pollination is modeled as the global search mechanism in the Flower Pollination Algorithm. This process is governed by Lévy flight, which characterizes long-distance probabilistic movements and enhances global exploration capability. In this context, Levy flight serves as the search operator that drives candidate solutions toward the best global solution. The mathematical formulation of the global pollination process is expressed in Eq. 2 as follows:

$$x_i^{k+1} = x_i^k + L(gbest - x_i^k) \quad (2)$$

Where ($i$) denotes the iteration index, ($k$) refers to the pollen particle index, ($gbest$) indicates the best global solution among all pollen particles ($x_i^k$), and ($L$) is the Levy factor governing the pollen transport during cross-pollination. The movement of pollen through the Levy factor is defined by a Levy distribution, which can be mathematically formulated in Eq. 3 as follows:

$$L = \frac{\lambda \Gamma(\lambda).\sin\left(\frac{\pi\lambda}{2}\right)}{\pi} \frac{1}{S^{1+\lambda}} \quad (S \gg S^0 > 0) \tag{3}$$

Where (Γ(λ)) represents the standard Gamma function, applicable for step sizes (S>>S0>0). Based on empirical tuning through preliminary simulations, the Levy distribution parameter (λ) is commonly set to 1.5 to promote faster convergence and maintain a balanced exploration–exploitation trade-off.

**Rule 2:**

Abiotic or self-pollination is modeled as the local search mechanism in the Flower Pollination Algorithm. This process represents solution updates within a limited neighborhood of similar candidate solutions. The mathematical formulation of the local pollination step is expressed in Eq. 4 as follows:

$$x_i^{k+1} = x_i^k + \varepsilon(x_m^k - x_j^k) \tag{4}$$

where ($x_m^k$) and ($x_j^k$) are pollen particles from the same plant species, and (ε) is a local search factor uniformly distributed in the range [0,1]. Local pollination occurs among closely located flowers of the same species, while cross-pollination occurs among distant flowers of different species. The transition among local and global search processes is governed by the switch possibility parameter p ϵ [0,1]. In most applications, the value of possibility switch (p) is typically set to 0.8 to ensure effective optimization. The complete procedural steps for implementing the Flower Pollination Algorithm (FPA) in Maximum Power Point Tracking (MPPT) applications are illustrated in the flowchart shown in Figure 5.

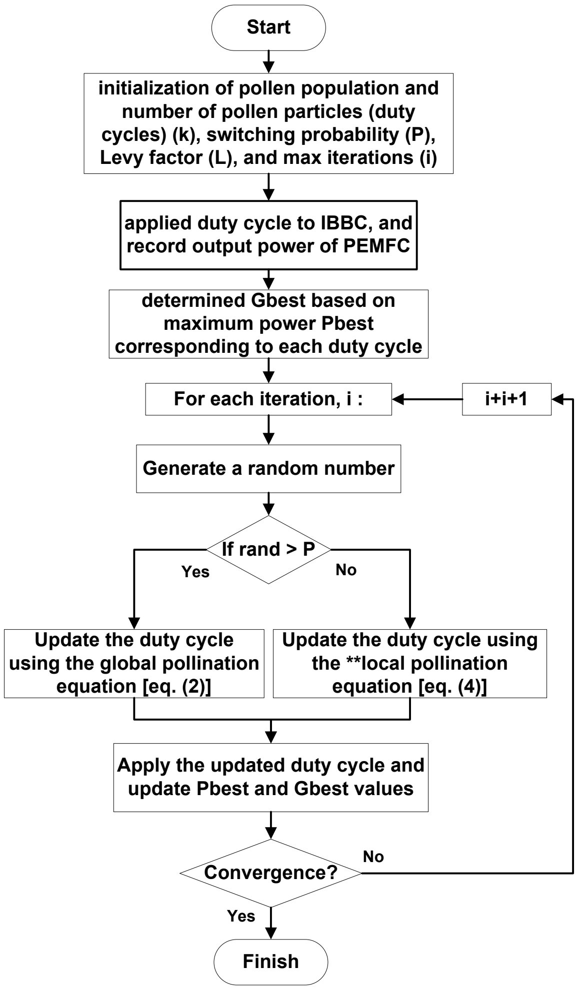


Figure 5. MPPT operation of the FPA Method

## 3. RESULTS AND DISCUSSION

The proposed system was evaluated through numerical simulations conducted in MATLAB R2023b. Four MPPT strategies were implemented and comparatively analyzed within the PEMFC framework: FPA, Cuckoo Search Algorithm (CSA), Fuzzy Inference System (FIS), and Particle Swarm Optimization (PSO).

To evaluate the accuracy and performance of the FPA method in comparison with other algorithms, five distinct simulation scenarios were analyzed:

Scenario 1 : Variation in cell temperature
Scenario 2 : Variation in membrane water content
Scenario 3 : Simultaneous variation in both membrane water content and cell temperature.

### 3.1. Modeling in Dynamic Cell Temperature

Proposed MPPT technique have been tested based on varying operational condition, particularly with changes in the cell temperature. During the simulation, the temperature increased from 303°K to 328°K, while the membrane water content was maintained constant at 14. The PEM fuel cell's maximum power output varied with temperature, achieving 1003 W at 303°K, 1083 W at 313°K, and 1190 W at 328°K, respectively.

The simulation scenarios for the MPPT methods are illustrated in Figures 6. Initially, the PEMFC works at cell temperature of 303°K. After ten seconds, the cell temperature increases to 313°K, and finally, further rises to 328°K after an additional 10 sec.

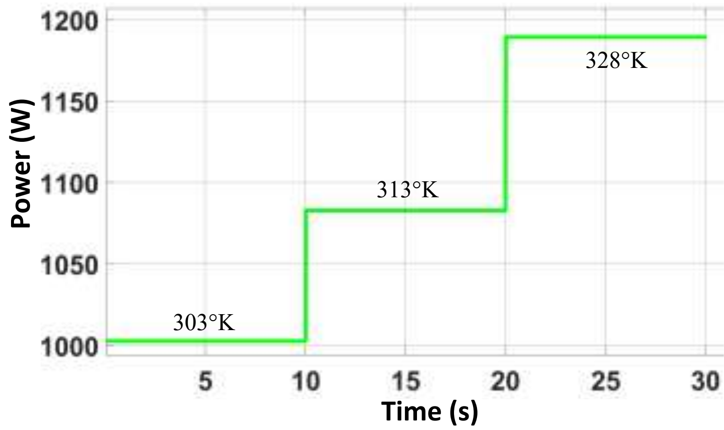


Figure 6. Pmax of PEMFC in various temperatures

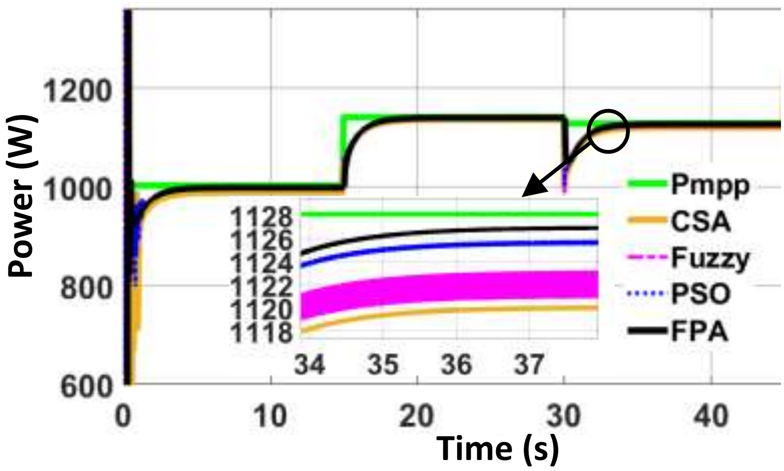


Figure 7. The MPPT result in Temperature Change

The application of a FPA method, as shown in Figure 7, yielded the output of PEMFC is 1000.3 W at 9 s, while the PEMFC's maximum power output was 1003 W. This corresponds to an error of 0.27% compared to the PEMFC's peak power. In the 2nd step, the produced PEMFC power was 1002.5 W at 9 s, achieving an error of 0.05%. Finally, in the third case, during the last interval, the generated power was 1002.2 W at 9 s, resulting in an error of 0.08%. The comprehensive simulation results obtained from the FPA method and other comparative MPPT algorithms are summarized in Table 2.

Table 2. Power error when temperature change

ISSN: 2715-6427

| MPPT Techniques | FPA | CSA | Fuzzy | PSO |
|---|---|---|---|---|
| Error at (%) | | | | |
| T= 303°K | 0.27 | 1.38 | 1.66 | 0.71 |
| T= 313°K | 0.05 | 0.73 | 0.73 | 0.23 |
| T= 328°K | 0.08 | 0.24 | 0.21 | 0.08 |
| Settling Time (s) | | | | |
| T= 303°K | 9 s | 9.5 s | 8 s | 8.2 s |
| T= 313°K | 9 s | 9.5 s | 8.5 s | 8 s |
| T= 328°K | 9 s | 9.5 s | 8.5 s | 8 s |
| Fluctuation (%) | 0.01 | 0.01 | 0.28 | 0.02 |

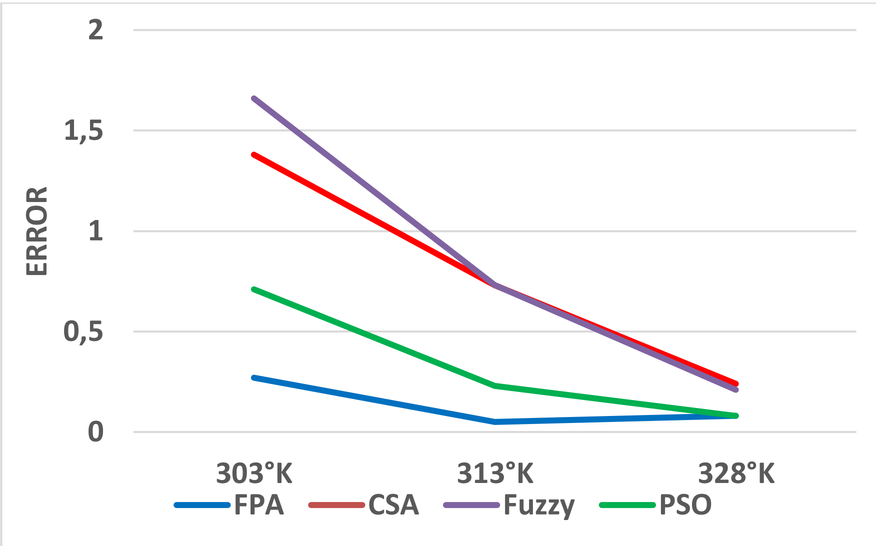


Figure 8. The Error graph of FPA when temperature change

The outcomes presented in Fig. 8 and Table 2 indicate that the presented FPA technique demonstrates inferior error and a faster response in achieving optimum power under varying temperature conditions. Whereas, the PSO technique also show error that fluctuates, but lower compared to the FPA method. Fuzzy and CSA have higher error than FPA and PSO methods. FPA Method also has lower power fluctuations compared with fuzzy and PSO method.

### 3.2. Modeling with Dynamic Membrane Water Saturation

To further evaluate the effectiveness of the presented approach, the FPA-based MPPT was tested under varying membrane water content conditions. Three hydration levels were considered, namely $\lambda = 13$, $\lambda = 14$, and $\lambda = 15$, while the cell temperature was maintained constant at 303 K.

As illustrated in Fig. 9, the maximum output power increases with membrane hydration, yielding 947 W at $\lambda = 13$, 1003 W at $\lambda = 14$, and 1058 W at $\lambda = 15$. These results confirm the sensitivity of the PEMFC power characteristics to membrane water content and highlight the necessity of adaptive MPPT control.

Initially, the PEMFC works when $\lambda = 14$. At $t = 15$ s, hydration level increases to $\lambda = 15$, and subsequently decreases to $\lambda = 13$ at $t = 30$ s. The corresponding dynamic responses of system using FPA and comparative MPPT techniques were presented in Fig. 9.

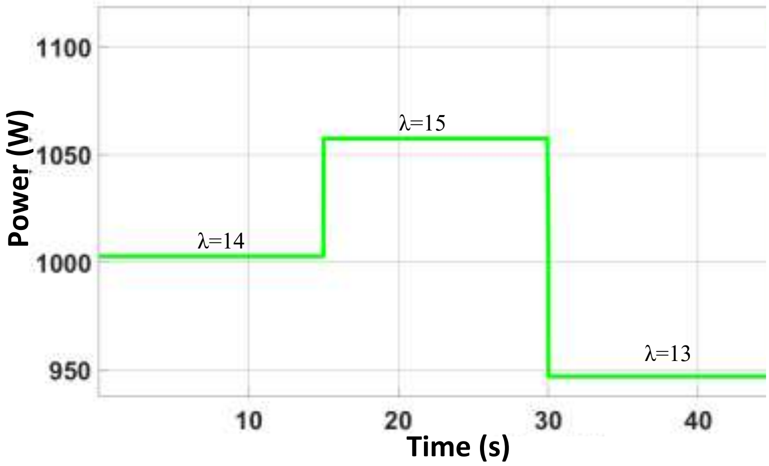


Figure 9. Pmax of PEMFC in various membrane water content

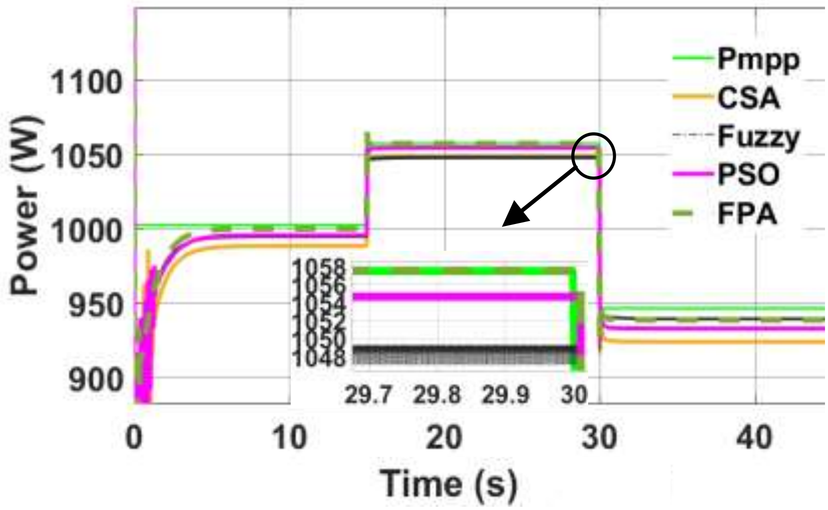


Figure 10. Pmax of PEMFC in various membrane water content

The result of simulation with FPA method produced the output power of 1000.2 W at 9 s, while the PEMFC's peak power output was 1003 W, resulting in an error of 0.27%. When 2nd step, the power produced was 1058 W at 1 s, and finally, the generated power was 938.6 W at 2 s. The total simulation findings employing the FPA and other approaches are displayed in Table 3.

Table 3. Power error when the membrane water content change

| MPPT Techniques | FPA | CSA | Fuzzy | PSO |
|---|---|---|---|---|
| Error at (%) | | | | |
| λ = 14 | 0.27 | 1.38 | 0.77 | 0.69 |
| λ = 15 | 0.26 | 0.79 | 0.80 | 0.32 |
| λ = 13 | 0.89 | 2.32 | 0.75 | 1.53 |
| Settling Time (s) | | | | |
| λ = 14 | 9 | 10 | 10 | 9 |
| λ = 15 | 1 | 3.5 | 3 | 2 |
| λ = 13 | 2 | 3.5 | 4 | 3 |
| Fluctuation (%) | 0.02 | 0.02 | 0.1 | 0.02 |
| Overshoot (%) | 2.47 | 1.48 | 2.73 | 3.28 |

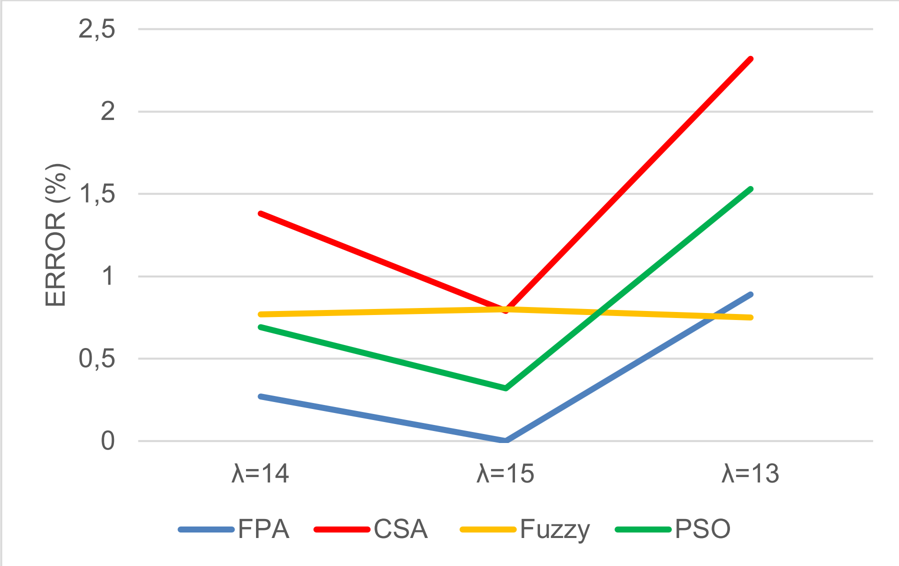

Figure 11. Error graph of FPA when various membrane water content change

As seen on table 3 and fig. 11, it can be observed that based on dynamic membrane water content values, the optimum power produced utilizing FPA technique was higher and faster. However, the power fluctuations produced by the FPA method remain greater than those of the other techniques.

### 3.3. Modeling with Dynamic Temperature and Membrane Water Content

Presented FPA method was tested further under dynamic variations of both membrane water content and cell temperature. Initially, the system operates at 303°K with a membrane water content of 14. At 10 sec, these parameters change to 15 and 313°K, and, finally, the membrane water content and temperature shift to 13 and 328°C, individually. Each condition produces the optimum power output of 1003 W, 1140.8 W, and 1129 W, as depicted in Fig. 12.

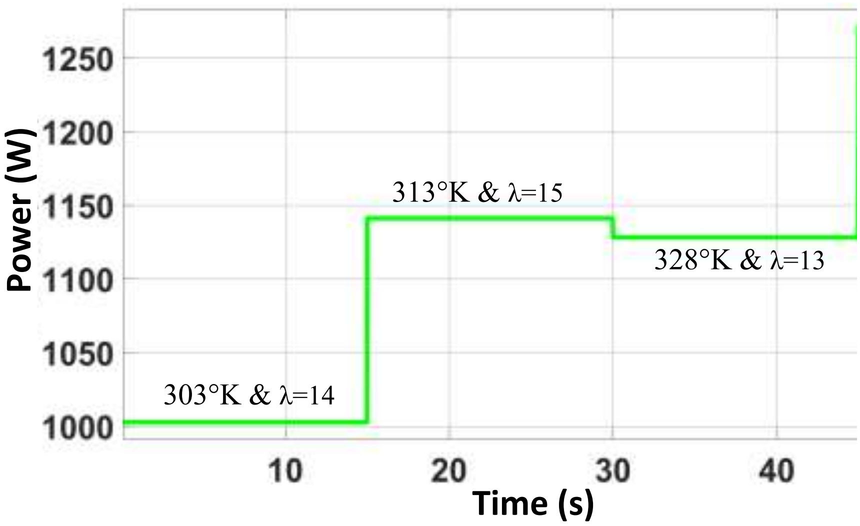

Figure 12. Pmax of PEMFC in various membrane water content and temperature

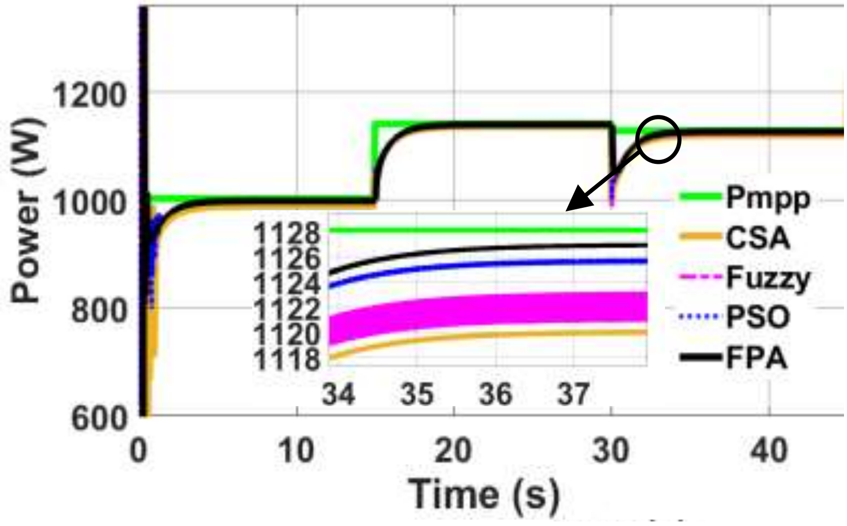


Figure 13. The MPPT result in membrane water content and temperature Change

The total simulation findings employing FPA and other approaches were displayed in Figure 13. The FPA method generated power outputs of 998.5 W, 1139.8 W, and 1127 W for scenarios 1 through 3, respectively. A comprehensive simulation differentiation outcomes among FPA technique and alternative techniques is summarized in the corresponding table 4

Table 4. Power error at dynamic Temperature and membrane water content change

| MPPT Techniques | FPA | CSA | Fuzzy | PSO |
|---|---|---|---|---|
| Error at (%) | | | | |
| λ=14 & 30°C | 0.45 | 1.38 | 1.66 | 0.7 |
| λ=15 & 40°C | 0.11 | 0.38 | 0.36 | 0.11 |
| λ=13 & 55°C | 0.18 | 0.71 | 0.53 | 0.3 |
| Settling Time (s) | | | | |
| λ=14 & 30°C | 12 | 12 | 9.5 | 10 |
| λ=15 & 40°C | 11 | 12 | 9 | 9 |
| λ=13 & 55°C | 6 | 13.5 | 9 | 6 |
| Fluctuation (%) | 0.1 | 0.01 | 0.2 | 0.02 |
| Overshoot (%) | 6 | 5.53 | 11.9 | 5.86 |

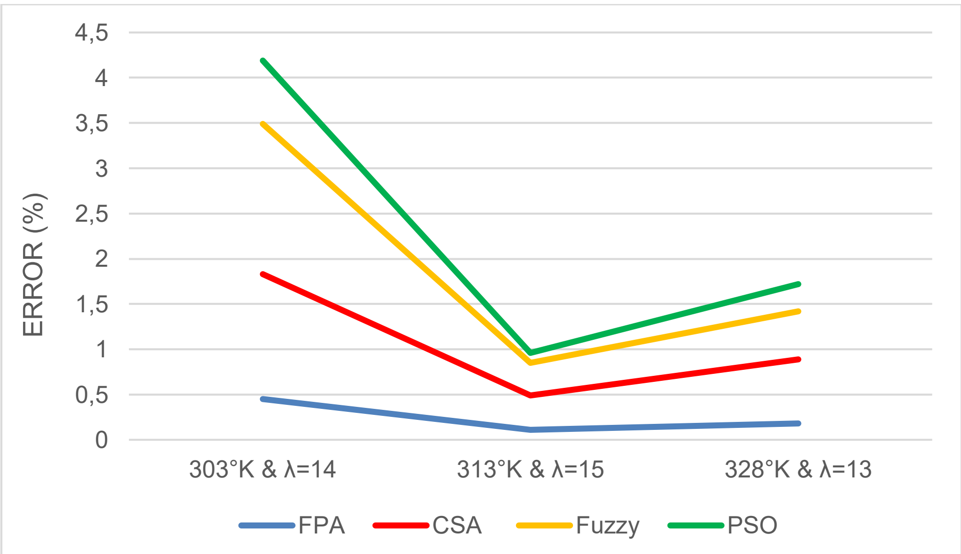


Figure 14. Error graph of FPA when various membrane water content and temperature change

It can be observed, as shown in figure 14 and table 4, that the FPA method generates higher power output, but still slower to achieves settling time under variations in temperature and membrane water content. However, in this scenario, the FPA method exhibits greater power fluctuations and overshoot than both the CSA and PSO methods.

## 4. CONCLUSION

This study proposes a FPA-based MPPT scheme to enhance the power extraction capability of Proton Exchange Membrane Fuel Cells (PEMFCs) based on dynamic conditions, including changes in membrane water content and stack temperature. The proposed approach determines the optimal duty cycle of an interleaved buck–boost converter (IBBC) to maintain operation at the maximum power point. Four working conditions were tried through simulation to evaluate the tracking accuracy and dynamic achievement of the technique. The results indicate that the FPA-based MPPT fulfilled zero steady-state error under dynamic membrane hydration and attains the quickest settling time of 1 s among the compared methods. Comparative analysis further demonstrates improved accuracy and dynamic response relative to existing MPPT techniques like as PSO, Fuzzy or CSA with lowest error 0.05%. Overall, the integration of FPA with the IBBC topology effectively enhances power extraction efficiency, tracking precision, and transient performance in PEMFC systems.

## ACKNOWLEDGEMENTS

The author would like to express the deepest gratitude to the Higher Education, Research, and Development Assembly of PP Muhammadiyah for their funding support for this research through the RISETMU funding mechanism under the Fundamental Research Collaboration scheme, with contract number 0259.811/I.3/D/2025.

## REFERENCES

[1] N. P. Ang, Tze-Zhang, Mohamed Salem, Mohamad Kamarol, Himadry Shekhar Das, Mohammad Alhuyi Nazari, “A comprehensive study of renewable energy sources: Classifications, challenges and suggestions,” *Energy Strateg. Rev.*, vol. 43, no. September 2022, p. 100939, 2022, doi: https://doi.org/10.1016/j.esr.2022.100939.

[2] M. M. Khaleel, Z. Yusupov, M. Güneşer, and A. Alsharif, “Effect of Fuel Cells on Voltage Sag Mitigation in Power Grids Using Advanced Equilibrium Optimizer and Particle,” *Jordan J. Electr. Eng.*, vol. 9, no. 2, pp. 175–188, 2023, doi: 10.5455/jjee.204-1669996684.

[3] A. Quteishat, M. A. Younis, A. A. Badr, A. Khezerlou, and A. Safari, “Salp Swarm Algorithm-Based Fractional Order PID Controller,” *Jordan J. Electr. Eng.*, vol. 10, no. 4, pp. 541–562, 2024, doi: 10.5455/jjee.204-1697828072.

[4] and P. F. Cigolotti, Viviana, Matteo Genovese, “Comprehensive Review on Fuel Cell Technology for Stationary Applications as Sustainable and Efficient Poly-Generation Energy Systems,” *Energies*, vol. 14, no. 16, p. 4963, 2021, doi: https://doi.org/10.3390/en14164963.

[5] K. M. Moe, H. M. Aung, H. A. Thar, and Y. Y. Win, “Analysis of energy production design from grid-connected 40 MW large PV power plant,” vol. 6, no. 1, pp. 1–11, 2023, doi: https://doi.org/10.24036/teknomekanik.v6i1.18972.

[6] J. Y. E. Y. U. N. Fam, S. Y. Wong, S. Member, K. B. Lias, S. Mekhilef, and S. Member, “Predictive Maximum Power Point Tracking for Proton Exchange Membrane Fuel Cell System,” *IEEE Access*, vol. 9, no. Ic, pp. 157384–157397, 2021, doi: 10.1109/ACCESS.2021.3129849.

[7] V. Karthikeyan, “Implementation of MPPT Control in Fuel Cell Fed High Step up Ratio DC-DC Converter,” in *2018 2nd IEEE International Conference on Power Electronics, Intelligent Control and Energy Systems (ICPEICES)*, IEEE, 2018, pp. 689–693. doi: 10.1109/ICPEICES.2018.8897443.

[8] N. Naseri *et al.*, “Proton Exchange Membrane Fuel Cell Modelling and Power Control by P & O Algorithm,” in *2018 6th International Renewable and Sustainable Energy Conference (IRSEC)*, IEEE, 2018, pp. 1–5. doi: 10.1109/IRSEC.2018.8703002.

[9] E. M. Barhoumi, “MPPT Control of an Interleaved Boost Converter for a Polymer Electrolyte Membrane Fuel Cell Applications,” in *2020 International Conference on Electrical and Information Technologies (ICEIT)*, Rabat, Morocco, 2020, pp. 2–6. doi: 10.1109/ICEIT48248.2020.9113228.

[10] H. Rezk and A. Fathy, “Performance Improvement of PEM Fuel Cell Using Variable Step-Size Incremental Resistance MPPT Technique,” *Sustainability*, vol. 12, no. 14, p. 5601, 2020, doi: https://doi.org/10.3390/su12145601.

[11] D. N. Luta and A. K. Raji, “Fuzzy Rule-Based and Particle Swarm Optimisation MPPT Techniques for a Fuel Cell Stack,” *Energies*, vol. 12, no. 5, p. 936, 2019, doi: 10.3390/en12050936.

[12] T. Hai, A. K. Alazzawi, and J. Zhou, “Performance improvement of PEM fuel cell power system using fuzzy logic controller-based MPPT technique to extract the maximum power under various conditions,” *Int. J. Hydrogen Energy*, vol. 48, no. 11, pp. 4430–4445, 2023, doi: https://doi.org/10.1016/j.ijhydene.2022.10.103.

[13] L. Fan and X. Ma, “Maximum power point tracking of PEMFC based on hybrid artificial bee colony algorithm with fuzzy control,” *Sci. Rep.*, vol. 12, p. 4316, 2022, doi: 10.1038/s41598-022-08327-5.

[14] S. A. Ansari *et al.*, “Modeling and Simulation of a Proton Exchange Membrane Fuel Cell Alongside a Waste Heat Recovery System Based on the Organic Rankine Cycle in MATLAB / SIMULINK Environment,” *Sustainability*, vol. 13, no. 3, p. 1218, 2021, doi: https://doi.org/10.3390/su13031218.

[15] P. Perdana and S. Saputra, “PEM Fuel Cell Power Control with Single Phase Inverter Connected To Distribution Grid Using Hysteresis Current Control Method,” *2022 Int. Semin. Intell. Technol. Its Appl.*, pp. 466–472, 2022, doi:

10.1109/ISITIA56226.2022.9855310.

[16] P. P. S. Saputra, M. Ashari, and Feby A. Pamuji, "Maximum Power Point Tracking of PEM Fuel Cell with Interleaved Buck Boost Converter Using Jellyfish Search Algorithm," *Intell. Networks Syst. Soc.*, vol. 18, no. 5, pp. 171–186, 2025, doi: 10.22266/ijies2025.0630.13.

[17] A. D. Majid Hosseinpour, Tooraj Sabetfar, "Power Conditioner Design and Control for a Grid-Connected Proton Exchange Membrane Fuel Cell," *Jordan J. Electr. Eng.*, vol. 9, no. 1, pp. 98–124, 2023, doi: 10.5455/jjee.204-1665256518.

[18] B. N. Alajmi and M. I. Marei, "Multiphase Interleaved Converter Based on Cascaded Non-Inverting Buck-Boost Converter," *IEEE Access*, vol. 10, pp. 42497–42506, 2022, doi: 10.1109/ACCESS.2022.3168389.

[19] A. T. G. Ali Zulfikaroglu, "Ripple and Passive Components Reduction on All SiC Multi-Device Interleaved Boost Converter for Hybrid Electric Vehicles," *Jordan J. Electr. Eng.*, vol. 9, no. 4, pp. 607–617, 2023, doi: 10.5455/jjee.204-1680506910.

[20] P. P. Surya, D. Irawan, and M. Zuhri, "Review and Comparison Of DC-DC Converters For Maximum Power Point Tracking System In Standalone Photovoltaic ( PV ) Module," in *2017 International Conference on Advanced Mechatronics, Intelligent Manufacture, and Industrial Automation (ICAMIMIA)*, IEEE, 2017, pp. 242–247. doi: 10.1109/ICAMIMIA.2017.8387595.

[21] I. Laoprom and S. Tunyasrirut, "Design of PI Controller for Voltage Controller of Four-Phase Interleaved Boost Converter Using Particle Swarm Optimization," *J. Control Sci. Eng.*, vol. 2020, no. 1, pp. 1–13, 2020, doi: https://doi.org/10.1155/2020/9515160.

[22] X. Mergos, P.E., Yang, "Flower pollination algorithm parameters tuning," *Soft Comput*, vol. 25, pp. 14429–14447, 2021, doi: ). https://doi.org/10.1007/s00500-021-06230-1.

[23] S. Lalljith, I. Fleming, U. Pillay, and K. Naicker, "Applications of Flower Pollination Algorithm in Electrical Power Systems : A Review," vol. 10, 2022.

[24] S. A. Eissa, S. W. Shneen, and E. H. Ali, "Flower Pollination Algorithm to Tune PID Controller of TCP / AQM Wireless Networks," vol. 4, no. 2, pp. 149–156, 2023, doi: 10.18196/jrc.v4i2.17533.

[25] Jahid, Ehtesham, M., Kirmani, S. et al., "Application of Flower Pollination Algorithm and its Comparative Analysis for MPPT of Solar Panels Under Partial Shading Conditions," *J. Inst. Eng. Ser. B*, vol. 106, pp. 1829–1842, 2025, doi: https://doi.org/10.1007/s40031-025-01197-1.

[26] J. K. Roland Kobla Tagayi, Jongbok Baek, "Flower pollination global peak search algorithm for partially shaded solar photovoltaic system," *J. Build. Eng.*, vol. 66, p. 105818, 2023, doi: https://doi.org/10.1016/j.jobe.2022.105818.

[27] H. S. R. M.M. Samy, S. Barakat, "A flower pollination optimization algorithm for an off-grid PV-Fuel cell hybrid renewable system," *Int. J. Hydrogen Energy*, vol. 44, no. 4, pp. 2141–2152, 2019, doi: https://doi.org/10.1016/j.ijhydene.2018.05.127.